WAAS-Based Threat Monitoring for a Local Airport Monitor (LAM) that Supports Category I Precision Approach

Jason Rife*, Sam Pullen*, Todd Walter*, Eric Phelts*, Boris Pervan† and Per Enge*

*Stanford University; Palo Alto, CA 94305

†Illinois Institute of Technology; Chicago, IL 60616

Abstract—The Federal Aviation Administration has sponsored the development of a Local Airport Monitor (LAM) prototype designed to enable GPS-based precision-approach by leveraging the existing capabilities of the Wide Area Augmentation System (WAAS). The LAM transmits a lumped WAAS correction via a Local Area Augmentation System (LAAS) message. The broadcast error bounds for the LAM are stricter than those for WAAS in order to enable Category I Precision Approach with a 10 m Vertical Alert Limit (VAL). The LAM ensures integrity of these tightened error bounds by leveraging both local monitoring and WAAS monitoring. This paper describes the use of WAAS monitoring to protect LAM users from ionosphere, code-carrier divergence and signal deformation threats. Although the LAM rebroadcast slightly delays the arrival of WAAS alerts to users, monitor integrity can nonetheless be ensured by restricting the allowed design space for user receivers.

I. INTRODUCTION

The Local Airport Monitor (LAM) effort aims to develop a GPS-based precision-approach system by leveraging the existing capabilities of the Federal Aviation Administration's Wide Area Augmentation System (WAAS). The proposed LAM architecture retransmits WAAS pseudorange corrections using the standard VHF Data Broadcast (VDB) message defined for the Local Area Augmentation System (LAAS). This architecture exploits the existing pseudorange corrections from WAAS but tightens the WAAS error bounds to support a 10 m Vertical Alert Limit (VAL) by validating the WAAS corrections with local measurements. Because the LAM architecture exploits operational technologies in the WAAS system and already certified LAAS user equipment, LAM has potential for inexpensive and rapid deployment when compared to CAT I LAAS.

LAM integrity requires that error bounds apply not only under nominal conditions but also under fault scenarios. Among the most dangerous fault conditions are those which introduce large differential ranging errors that are either fully or partially unobservable to LAM. (Examples of these include steep ionosphere gradients, GPS C/A-code signal deformation, and satellite code-carrier divergence). Rather than incorporating specialized hardware and monitoring algorithms to detect these fault modes locally, the LAM system relies on external monitoring algorithms that either already exist within WAAS or that will be added to WAAS by the end of 2008.

The use of external monitoring introduces both benefits and liabilities for the LAM architecture. On the positive side, substituting WAAS-based monitors for specialized local monitors keeps LAM complexity low. Furthermore, the wide baselines and dense monitoring network of WAAS provide greater sensitivity for fault-mode detection than an isolated local monitor could provide. Not all of the features of external monitoring are advantageous to LAM, however. In particular, the time delay associated with the reception and rebroadcast of the WAAS message introduces a significant challenge in meeting the 6-second time-to-alarm requirement for Category I approaches. Also, because WAAS does not broadcast specific monitor flags but only more general indications of system health, LAM continuity and availability suffer slightly.

This paper details WAAS-based monitors for three significant fault-modes that impact LAM integrity: anomalous ionosphere gradients, satellite Signal Deformation (SD), and satellite Code-Carrier Divergence (CCD). In order to detect these fault modes, the LAM ground facility monitors WAAS integrity parameters including the User Defined Ranging Error (UDRE) and the User Ionosphere Vertical Error (UIVE). Analysis and data presented in the paper demonstrate that the WAAS-based monitors provide full integrity to LAM users even in the event of severe threats. This monitoring approach, moreover, is valid for both Position-Domain Monitoring on the Ground [1] and Position-Domain Monitoring in the Air [2].

II. THREAT DESCRIPTION

This section describes three major threats for which LAM relies on external monitoring: (1) ionosphere gradients, (2) CCD, and (3) SD.

A. Ionosphere Threats

Ionosphere spatial decorrelation anomalies have been studied in great detail by both WAAS and LAAS since unusually large decorrelations were discovered in WAAS supertruth data from the ionosphere storm of April 6 – 7, 2000 [3]. Under active ionospheric conditions, anomalous ionospheric gradients may exist that result in errors large enough to cause loss of integrity for the user aircraft. Under these circumstances ionosphere monitoring is deemed necessary in LAAS and LAM.

A threat model for ionospheric gradients was developed based on WAAS Super Truth data analysis. The threat model represents anomalous spatial ionospheric delay differences with a piecewise linear function, shown below. Note that this linear model of the wavefront is a simplification of reality. Although nonlinear effects appear in the time series of the anomaly, this model suffices to estimate the threat.

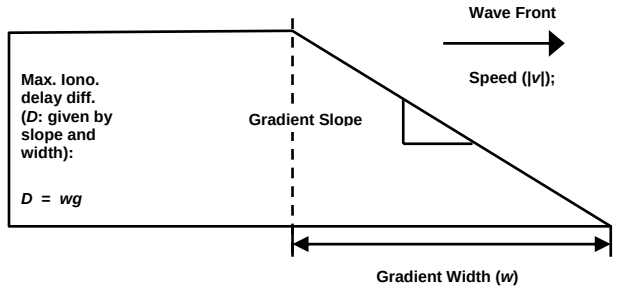

Fig. 1. Threat Model of Anomalous Ionosphere Gradient

This piecewise linear model is described by three parameters.

- Gradient speed (|v|) measured in m/s
- Gradient width (w) measured in km
- Gradient slope (g) measured in mm/km

The maximum delay (D) introduced as a result of this gradient is defined as the product of the gradient width and slope (D = wg). Bounds for each value, as of August 2005, are given by [4]. These parameters reflect a rational analysis of observed gradients in all data currently analyzed with some conservatism added. It is recognized that safety of life operations require continued characterization of this phenomenon.

LAM mitigates the ionospheric gradient threat by exploiting the wide-baseline ionosphere monitoring capabilities of WAAS. Analysis of data for days with nominal and active ionosphere conditions indicates that threatening gradients only arise during severe ionosphere storms. Thus, if WAAS detects a storm-affected region, LAM can protect its users by denying satellites that lie in the storm region.

B. Code-Carrier Divergence Threats

Code-Carrier Divergence (CCD) occurs when the clock reference for the GPS code drifts away from that of the underlying carrier signal. Nominal ionosphere activity causes mild CCD. Although the LAM error bound is designed to account for this activity, a rare satellite fault could introduce much larger CCD errors. In this fault mode, it is hypothesized that the satellite code generator could drift away from the underlying carrier signal. This failure has not been observed in GPS operations to date, but satellite-induced CCD is considered a sufficient hazard to warrant fault monitoring.

The CCD error transient is tied to the design of carrier-smoothing filters implemented in WAAS, in the LAM ground facility and in the user receiver. The standard form of the carrier-smoothing filter for these systems is given by the following equation, which blends measurements of pseudorange, ρ, with accumulated carrier-phase, ϕ, to produce a smoothed pseudorange estimate, P, at each epoch, n. Carrier-phase measurements are scaled by the carrier wavelength, λ, and filtered by a weighting coefficient, $\alpha = 0.005$, which gives a nominal filter time constant of 100 s for 2 Hz sampling.

$$P_n = \alpha\rho_n + (1-\alpha)\left(P_{n-1} + \frac{\lambda}{2\pi}(\phi_n - \phi_{n-1})\right) \quad (1)$$

When divergence occurs, the transmitted code and carrier signals may drift away from the nominal clock reference. If the drift rate for the code is $d_{n,\rho}$, and if the drift rate for the carrier is $d_{n,\phi}$, then these errors impact pseudorange smoothing as follows.

$$\begin{aligned} P_{n,CCD} &= \alpha\left(\rho_n + d_{n,\rho}\Delta t\right) \\ &\quad + (1-\alpha)\left(P_{n-1} + \frac{\lambda}{2\pi}(\phi_n - \phi_{n-1}) + d_{n,\phi}\Delta t\right) \end{aligned} \quad (2)$$

The error from ground smoothing at each time step is Δg_n.

$$\Delta g_n = P_{n,CCD} - P_n = \alpha d_{n,\rho}\Delta t + (1-\alpha) d_{n,\phi}\Delta t \quad (3)$$

The magnitude and sign of the divergence terms, $d_{n,\rho}$ and $d_{n,\phi}$, depend on the source of the CCD. The physics of ionosphere-induced CCD, for instance, produces equal and opposite divergence terms ($d_{n,\rho} = -d_{n,\phi}$). For satellite-induced CCD, the code-phase generator is assumed to drift at a constant rate relative to the satellite clock ($d_{n,\rho}$ is constant and $d_{n,\phi} = 0$).

For analysis purposes, it is both conservative and convenient to convert the CCD error model from the discrete domain, as

described by (3), into the continuous domain. The following differential equation bounds the time evolution of the CCD ground-filtering error, g. Here the satellite-induced CCD drift starts at time zero with a constant rate, $d = |d_{n,\rho}|$. The carrier-smoothing filter time-constant (nominally 100 s) is labeled τ_{cs}.

$$\tau_{cs}\dot{g} + g = \begin{cases} 0 & t \le 0 \\ t \cdot d & t > 0 \end{cases} \quad (4)$$

For the case of a 100-s time constant, this first-order LTI filter results in the ramp response illustrated in Fig. 2. In the figure, the filtered and raw error values are normalized by the divergence magnitude, d. At steady-state, the filtered error converges to a constant offset, $d\tau_{cs}$, below the input measurement ramp. The CCD threat model allows the parameter d to take any positive value.

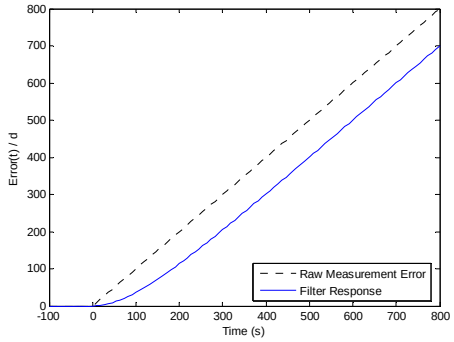

Fig. 2. Smoothing-Filter Response to Ramp Divergence Error Input

In principle, the user filter response, $u(t)$, would be identical to the ground response, $g(t)$, such that the net differential error, $E(t)$, would be zero for the CCD fault mode. In practice, these two terms do not necessarily cancel, and they may leave a differential error given by the following equation, which conservatively assumes full convergence for the ground filter.

$$E(t) = u(t - t_a) - g(t) \quad (5)$$

In this equation, the user transient may not match the ground's because of a tracking restart (at a time, t_a), transmission latency , or the designed ramp response of the user filter. The differences between u and g may be decomposed into two parts which are either observable or unobservable to the LAM ground station. Errors caused by design differences of the user receiver or by a user tracking restart are unobservable at the LAM ground station. Errors associated with the six-second latency of the differential correction transmitted by WAAS, by contrast, are observable in the WAAS decision statistic. Although observable CCD errors may reach several meters in magnitude, LAM inherently protects observable errors through its Vertical Protection Level (VPL) expression. Thus, WAAS monitoring is necessary only to protect those errors otherwise unobservable at the ground station.

Error transients that result from differences in carrier-smoothing filter design or from a tracking restart are illustrated in Fig. 3. In each plot, the dotted function represents the nominal ramp error caused by CCD. The blue solid function represents the ground CCD ramp response, described by (4). The red dashed function represents modified user responses both for an unmatched filter design (left) and for a filter restart (right). All curves have been normalized by the divergence rate, d. The differential error, $E(t)$, between the ground station and the user is illustrated in Fig. 4. Because the user filter, u, is required to match the nominal LAAS filter, g, within a 100 s period after a restart event (see Section V), CCD faults are only considered threatening shortly after a user filter restart (t_a > -100 s).

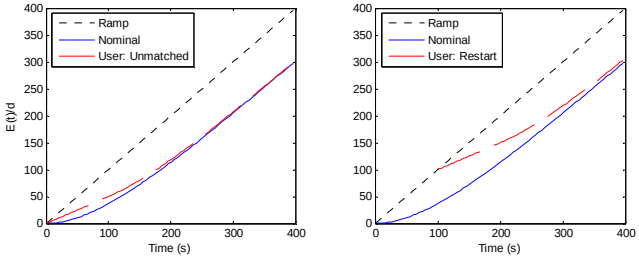

Fig. 3. Smoothing-Filter Differential Error due to User-Filter Design Differences (left) and User-Filter Restarts (Right)

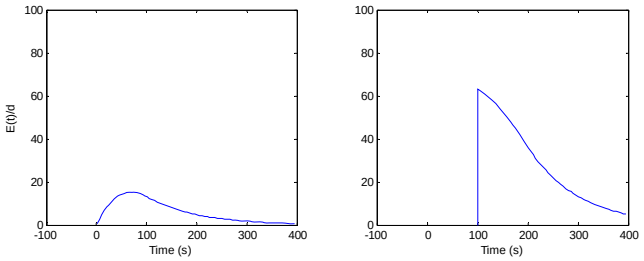

Fig. 4. Unobservable Differential Errors due to Unmatched User-Filter Ramp Response (left) and due to User-Filter Restart (Right)

C. Signal-Deformation Threats

SD events occur when the electronics onboard a GPS satellite distort the shape of the chips in the broadcast code sequence. These distortions change the shape of the correlator peak observed by a GPS receiver and, in effect, lengthen or shorten the measured pseudorange. Different GPS receivers experience different correlator peak distortions when exposed to the same threat. Consequently, a differential correction system, such as LAM, cannot issue pseudorange corrections that completely remove the SD perceived by different users.

Fortunately, SD is rare. To date only one SD event has ever been detected. This fault was observed for satellite SV19 in October of 1993. It is not known when the fault first occurred, and it is possible that the fault was present from the time the satellite was launched. To be conservative, however, the threat model assumes that an instantaneous transition between faulted and unfaulted conditions is possible.

The size of the SD error varies over the user-receiver design space and the signal-deformation threat space. The user design space is restricted for LAM, as discussed in Section V. The signal-deformation threat space is identical to that for LAAS and WAAS and is modeled using three parameters [5]. These three parameters consist of damped natural frequency (f_d), damping constant (σ), and discrete lead/lag (Δ). The standard threat model assumes f_d falls in the 4-17 MHz range for analog faults or in the 8-12 MHz for combined analog/digital faults. The threat model bounds the damping constant, σ, in the range of 0.8-8.8 nepers/chip. If a digital fault is present, Δ is limited to a lead/lag of ±0.12 chip.

Based on specific models for the user and threat spaces, the maximum user-to-ground differential error can be computed in simulation, and verified in experiment. This document relies on a simulation that uses a detailed model of receiver physics to derive the steady-state receiver error associated with any point in the combined threat and user parameter spaces [5]. As with the case of the satellite CCD fault, these errors may be partially observable. Deformation errors that result from differences in the user and ground receivers or from a user tracking restart are not generally observable. In theory, SD errors could be substantially reduced by matching the ground and user receivers; however, matching is generally not practical, as SD errors are highly sensitive to precise design tolerances for the analog components of GPS receivers. As such, all differential errors between the WAAS corrections and the user receiver are treated as unobservable to the LAM receiver.

Fig. 5 illustrates the magnitude of the LAM differential SD errors, E_{ss}. Each point on the figure represents one of approximately 15,000 discretized regions from the SD threat space. These error levels include inflation that compensates for latency between the broadcast of the WAAS differential corrections and their arrival at the user receiver. Inflation is minimal, since the user and LAM ground station both update broadcast measurements with a range-rate correction [6], [7].

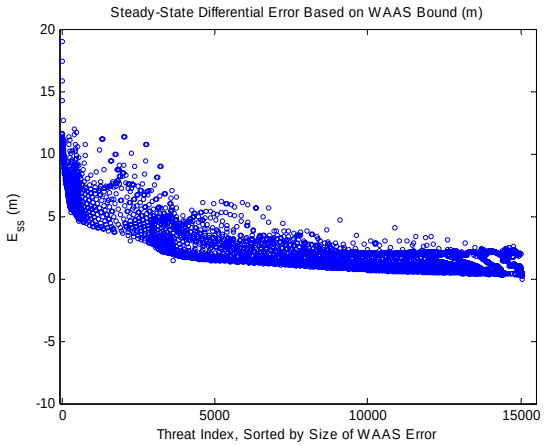

Fig. 5. SD Threat Space: Differential Error Accounting for Transmission Delay and Range-Rate Extrapolation

Based on these values of steady-state error, a bound on the differential-error transient, $E(t)$, is defined as a first-order LTI filter step response, where the steady-state error from Fig. 5 is E_{ss} and the filter time constant is τ_{cs}.

$$E(t) = E_{ss}\left(1\text{-}e^{-t/\tau_{cs}}\right) \quad \text{for } t > 0 \tag{6}$$

This differential error bound is based on the assumption of continuous satellite tracking. In practical operations, the user carrier-smoothing filter may start or restart when a satellite is rising above the horizon, when a cycle slip occurs, or when an aircraft maneuvers in such a way as to occlude one or more satellites in view. If such a restart occurs, the full signal-deformation error is immediately absorbed into the navigation solution. Thus the carrier-smoothing filter does not delay the onset of HMI if a user-filter restart occurs.

$$E(t) = E_{ss} \quad \text{for } t > 0 \tag{7}$$

Fortunately, the probability of a user restart occurring within a few seconds of the onset of SD is extremely low.

III. WAAS MONITORING ALGORITHMS

A. *WAAS Ionosphere Monitor*

To date, the only ionosphere monitor developed for conventional LAAS that detects all hazardous ionosphere gradients is a long-baseline monitor that requires reference stations sited 13-16 km apart along the aircraft approach path [8]. Although this type of monitor is not practical for conventional LAAS, LAM can obtain the benefits of long-baseline monitoring by leveraging WAAS.

WAAS interpolates measurements from its network of reference stations to define a grid-based ionosphere model for CONUS. An "ionosphere storm detector" checks each Ionosphere Grid Point (IGP) correction for insufficient "planarity." IGPs for which the degree of non-planarity crosses a pre-set chi-square threshold have their Grid Ionosphere Vertical Error (GIVE) set to a 3.29 σ_{GIVE} value of 45 meters and their GIVE Index (GIVEI) set to a value of 14, on a scale between 0 and 15. This value is too high to be useful for precision-approach applications. IGPs with insufficient measurements to assure the consistency of a planar fit have their GIVEI value set to 15, or "not monitored," to indicate that the ionosphere correction for this IGP cannot be guaranteed (see [7] for more details of the WAAS ISD algorithm). To protect LAM users from severe ionosphere gradients, IGPs with GIVEI values of 14 or 15 should be excluded by LAM.

These classifications should be revisited in the future, when WAAS introduces its new Extreme Ionosphere Storm Detector (EISD). In particular, it should be verified that the only ionosphere storms threatening to LAM are those deemed to be "extreme storms" by the WAAS EISD.

B. WAAS CCC Monitor

Conventional LAAS ground stations each implement a specialized measurement monitor to detect CCD. LAM simplifies certification by leveraging an existing monitor within WAAS designed for this function: the Code-Carrier Coherence (CCC) monitor. The CCC monitor measures the difference between WAAS corrections filtered with two different time constants, one short (25 s) and one long (2 hours). If the lack of coherence between the two signals grows larger than the monitor threshold, the CCC monitor triggers a flag that excludes the alarmed satellite.

Divergence faults are modeled as introducing a ramp function into both the short and long-duration filters. Because the long-duration filter response is negligible during the initial minutes of the divergence event, the CCC monitor transient is modeled as the ramp response for a first-order LTI filter with a 25-second time constant. The ratio of the monitor statistic transient, $m_{ccc}(t)$, to the divergence rate, d, is a function of the faster smoothing time, τ_{ccc} = 25 s.

$$\frac{m_{ccc}(t)}{d} = t - \tau_{ccc}\left(1 - e^{-t/\tau_{ccc}}\right) \tag{8}$$

A flag trips if the monitor statistic exceeds a preset threshold. The CCC monitor threshold is different for each satellite, with a value that depends on the number of WAAS Reference Equipment (WRE) receivers tracking that satellite.

The number of WREs is reflected in the WAAS broadcast parameter called the User Defined Ranging Error (UDRE). The UDRE Index (UDREI) ranges between 0 and 15. A higher UDREI indicates a smaller number of WREs tracking a particular satellite. The WAAS MOPS require that UDREI be no greater than 11 for a satellite used in precision approach. The CCC threshold, T_{CCC}, is defined in terms of the monitor noise sigma, which is $\sigma_{mon,ccc}$ = 0.7 m at UDREI = 11.

$$T_{ccc} = 12\sigma_{mon,ccc} \tag{9}$$

C. WAAS Signal Deformation Monitor

In LAAS, specialized receivers with multiple correlator spacings are required to detect SD events. LAM significantly reduces costs by leveraging the Signal Deformation Monitor (SDM) scheduled for installation as a WAAS upgrade in 2008. This capability will leverage specialized SD receivers installed at WAAS reference stations. Upon detection of SD, WAAS will transmit a message to warn users of the fault.

The WAAS monitor will function by computing metrics to assess the level of deformation in each satellite's correlation-peak. These metrics are compared to a threshold based on the number of active SDM receivers in WAAS. For worst-case, instantaneous SD, the monitor statistic transient is modeled as the filter response to a step-input function. The ratio of the monitor statistic transient, $m_{sdm}(t)$, to the size of the steady-state error, m_{ss}, is a function of the filter smoothing time, which is expected to be no slower than τ_{sdm} = 50 s.

$$\frac{m_{sdm}(t)}{m_{ss}} = 1 - e^{-t/\tau_{sdm}} \tag{10}$$

A flag trips if this monitor statistic exceeds a preset threshold. As with the CCC monitor, the WAAS UDREI and threshold are functions of the number of WREs available.

Two SDM threshold levels are considered in LAM analysis. SD threats pose a greater risk for LAM at higher elevations. Fortunately, more WREs are generally available to track higher elevation satellites, allowing for more sensitive fault detection (given a fixed false alarm rate). This tradeoff may be captured with minimal overconservatism by analyzing two thresholds, a tighter threshold associated with UDREI = 8 (for high elevation satellites) and a looser threshold associated with UDREI = 11 (for low elevation satellites). Satellites with UDREI $\geq$ 11 are not considered since the WAAS MOPS forbids their use in precision approach.

Although the WAAS SDM threshold has not been finalized, it will have a value no greater than six times $\sigma_{mon,sdm}$.

$$T_{sdm} = 6\sigma_{mon,sdm}\left(N_{WRE}\right) \tag{11}$$

As monitor noise is averaged over multiple WREs, the value of the monitor noise sigma, $\sigma_{mon,sdm}$, and hence of the threshold, T_{sdm}, depends on the number of WREs, N_{WRE}, viewing the faulted satellite. In this analysis, it is assumed that the sigma value is improved over the single-monitor noise level by a factor of 2.12 in the case of UDREI = 11 and by a factor of 2.74 in the case of UDREI = 8.

For SD integrity analysis, it is convenient to reduce the description for each threat in the discretized threat space to a parameter pair: E_{ss} (for the worst user) and m_{ss}. For any threat in the threat space, the value of m_{ss}, like the value of E_{ss}, can be determined through a physics-based simulation. The simulated SD threat space for LAM is characterized in Fig. 6 in terms of E_{ss} and m_{ss}. This threat space reflects the user-receiver restrictions of Section V.

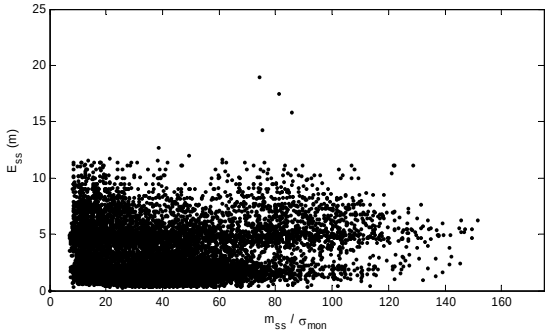

Fig. 6. Steady-State Error and Monitor Statistic Values for WAAS SDM

IV. LAM MONITORING ALGORITHMS

When a WAAS monitor excludes an affected satellite, WAAS guarantees that its users will receive the warning within six seconds of the epoch at which the fault-induced error becomes hazardous. LAM users will also receive this warning, though the six-second alert time is not inherently guaranteed. This section describes two additional algorithms by which LAM can guarantee a six-second alert time.

The two algorithms are called the UIVE and UDRE monitors. The UIVE monitor protects against ionosphere storms; the UDRE monitor protects against CCD and SD events. The block diagram of Fig. 7 indicates how these monitors integrate into LAM. A satellite must pass both monitors to be processed by the LAM carrier-smoothing filter.

A. UIVE Monitor

Although WAAS permits users to perform non-precision approach using storm-affected satellites, the LAM error bounds are too tight to permit operation with satellites that might be impacted by an ionosphere gradient. The LAM prevents users from navigating with these signals by applying a threshold to the WAAS ionosphere parameters for each satellite. Since threateninig gradients only appear when GIVEI reaches the top of its scale (values of 14 or 15), these index values could, in principle, be used as a conservative indicator of the possible presence of severe ionosphere gradients; however, standard WAAS receivers do not output grid data, but rather only a single, lumped ionosphere parameter for each satellite. Accordingly, the LAM ionosphere quality threshold is defined using this lumped parameter: the User Ionosphere Vertical Error (UIVE).

$$\begin{aligned} &\text{UIVE} \le 13.0 \text{ m; and} \\ &\text{IPP flag = "valid"} \end{aligned} \tag{12}$$

The UIVE is a lever-weighted average of the ionosphere sigmas at the four corners of a geographic grid cell. The rationale for the UIVE threshold and the IPP status flag test is developed in Section VI.

B. UDRE Monitor

WAAS does not provide differential corrections for satellites on which its monitors detect a CCD or SDM fault. The LAM inherently passes this protection on to its users. Because of alert time requirements, however, the LAM must apply additional screening to prevent use of satellites with loose monitoring thresholds. Loose thresholds indicate rising satellites which do not qualify for precision approach.

Thresholds become tighter as more WAAS receivers, abbreviated WAAS Reference Equipment (WREs), track a particular satellite. Since UDREI increases as the number of WREs tracking a satellite decreases, UDREI serves as a conservative indicator of WAAS monitor thresholds. In order to ensure system integrity, the LAM must apply the following UDREI cutoff, which is elevation dependent.

$$\text{UDREI} \le \begin{cases} 11, & el \le 38^\circ \\ 8, & el > 38^\circ \end{cases} \tag{13}$$

The integrity implications of (13), and of LAM restrictions on ground and user equipment, are discussed in Section VI.

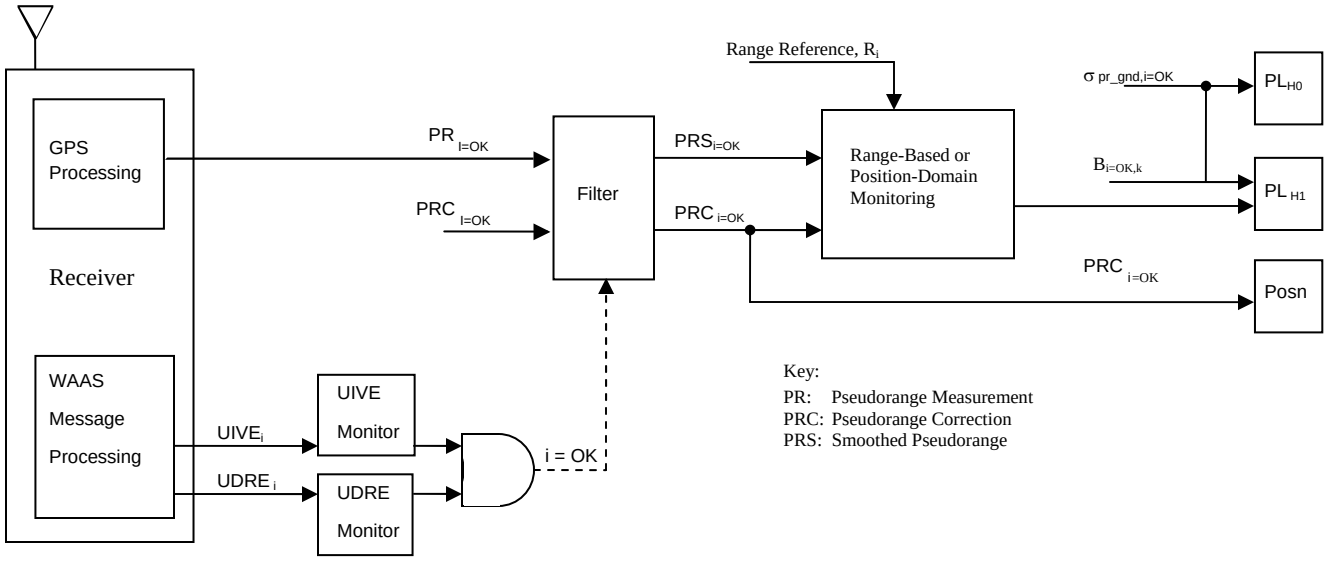

Fig. 7. LAM Block Diagram Including UIVE and UDRE Monitors

V. USER AND GROUND SEGMENT REQUIREMENTS

To achieve the six-second time-to-alert requirement for Category I, LAM places certain restrictions both on the LAM ground facility and on user receivers. No additional requirements (beyond those in the current LAAS MOPS [6]) are needed to mitigate the ionosphere gradient threat; however, some additional requirements are necessary to protect users from SD and CCD faults.

A. Ground System Requirements

In addition to obeying the UIVE and UDREI constraints (12) and (13), the LAM ground facility must also meet the following requirements in order to ensure system integrity. These constraints apply to parameters defined in prior papers [1, 2] and in the LAM Algorithm Description Document [9].

- *The LAM ground facility will only approve satellites that local receivers have tracked for at least 200 seconds.*
- *The Total-Transmission-Time (TTT) for a WAAS warning message to reach the airborne user must not exceed 10 seconds.* This budget includes the following allowances.
  - Collect/process data at WAAS Master Station: 4.8 s
  - From Master Station to LAM through Geo: 1.4 s
  - Process message at LAM: 0.8 s
  - From LAM to User, allowing for missed messages and user-receiver processing: 3 s
- *The LAM VPL must have a K_{bnd} value of at least 5.45.*
- *For CCD integrity, the minimum value of the true user ranging error, $\sigma_{pr,i}$, must be at least 0.2 m.* This error is the root-sum-square of the actual error associated with the ground monitor, with aircraft receiver noise, and with ionosphere and troposphere decorrelation noise.

$$\sigma_{pr,i} = \sqrt{\sigma_{gnd,i}^2 + \sigma_{air,i}^2 + \sigma_{iono,i}^2 + \sigma_{tropo,i}^2} \tag{14}$$

- *The evaluated user sigma must be large enough and the R_{max} value small enough to support SDM integrity, as specified by Table 1.* The evaluated user pseudorange sigma, $\tilde{\sigma}_{pr,i}$, for any satellite, *i*, is based on the broadcast values of the ground, ionosphere and troposphere error terms. The tilde superscripts indicate broadcast values, which may be inflated from the actual values of (14).

$$\tilde{\sigma}_{pr,i} = \sqrt{\tilde{\sigma}_{gnd,i}^2 + \sigma_{air,i}^2 + \tilde{\sigma}_{iono,i}^2 + \tilde{\sigma}_{tropo,i}^2} \tag{15}$$

The R_{max} factor describes the ratio of the true WAAS user error to the inflated user pseudorange sigma, $\tilde{\sigma}_{pr,i}$ [10].

$$R_{max} = \max \text{ over any } \theta \text{ of } \left\{ \frac{\sigma_{true,i}(\theta)}{\tilde{\sigma}_{pr,i}(\theta)} \right\} \tag{16}$$

The true WAAS user error sigma, $\sigma_{true,i}$, is modeled in [11].

TABLE 1. CONSTRAINTS ON $\tilde{\sigma}_{pr,i}$ AND R_{MAX}

Minimum $\tilde{\sigma}_{pr,i}$ above 38°	Minimum $\tilde{\sigma}_{pr,i}$ at or below 38°	Maximum R_{max}
0.38	0.48	0.85
0.41	0.51	0.96
0.44	0.58	1.07

B. User Receiver Requirements

In order to ensure integrity for LAM users, the user receiver design space must be constrained somewhat tighter than the LAAS and WAAS Minimum Operational Performance Standards [6], [7]. These additional constraints are necessary for LAM to meet the time-to-alert requirement for Category I.

- *For SDM integrity, front-end filter bandwidth for the user receiver must fall in the range of 15.5 – 16.5 MHz; chip spacing, in the range of 0.15 – 0.25 chip; and group delay in the range of ±50 ns.* This constraint is notably tighter than the user space for conventional WAAS and LAAS.
- *The step response of a time-varying user carrier smoothing filter must match the LTI filter described by the LAAS MOPS (Section 2.3.6.6) within 100 seconds of a restart event and must have a step response bounded between the response of the nominal LTI filter and the time-varying filter with time-constant equal to* $t - t_a$. This restriction limits the size of the error, $E(t)$, from (5).
- *The code-noise and multipath sigma term used for the aircraft receiver must be as large or larger than the value given by the AAD-B curve and must incorporate a term that bounds nominal divergence errors.* The requirement for a nominal divergence error term, $\sigma_{div,a}$, is consistent with the LAAS MOPS [6]. The airborne error sigma that combines the B-curve with the divergence sigma is given below as a function of elevation, *el*.

$$\sigma_{air} \geq \sqrt{\left(0.13+0.53e^{-el/10^\circ}\right)^2 + \left(0.11+0.13e^{-el/4^\circ}\right)^2 + \sigma_{div,a}^2 (t - t_a)} \tag{17}$$

The divergence error term is intended to protect the user from nominal ionospheric divergence in the event of a user smoothing-filter restart. This divergence bound is dependent on the user carrier-smoothing filter step response, $u(t - t_a)$, where t_a is the filter restart time.

$$\sigma_{div,a}(t - t_a) \geq 0.018 \cdot \left| 100 - u(t - t_a) \right| \tag{18}$$

VI. MONITOR INTEGRITY

For user receivers that meet the additional requirements of Section V, it is possible to prove that the LAM UDRE and UIVE monitors ensure the integrity of the user protection level and the time-to-alert requirement.

A. UIVE Monitor Integrity

In validating the integrity of ionosphere storm detection via the LAM UIVE monitor, the major integrity issue involves the definition of a threshold that operates on the lumped ionosphere parameter, UIVE, rather than the grid vertex parameters (GIVEI) for each satellite. Time-to-alert is a non-issue for ionosphere monitoring, since ionosphere storms develop slowly and since WAAS publishes a conservative ionosphere description which is valid for the entire 5 minute interval between successive ionosphere grid update messages.

Hazardous gradients may occur if the GIVEI value at an Ionosphere Grip Point (IGP) is 14 or 15. Fig. 8 shows an example of a potentially hazardous grid cell in which one IGP has a GIVEI value of 14 (which corresponds to a 45-meter GIVE sigma). This elevated GIVE level makes nearby LAM Ionosphere Pierce Points (IPPs) unsafe to use [4].

In Fig. 8 the GIVE values were selected to illustrate a worst-case grid cell in which all except the hazardous IGP have the minimum-possible GIVE value. This "floor" value has an associated GIVE sigma of 3.0 m (and a corresponding GIVEI = 9). For an IPP located roughly in the center of the cell, the resulting lumped UIVE is approximately the average of the four GIVE values; i.e., UIVE = 0.25 (3 + 3 + 3 + 45) = 13.5 m. Therefore, a UIVE threshold of 13 meters excludes all IPPs that are in the grid cell quadrant closest to a storm-region IGP (GIVEI = 14).

GIVEI values of 15 ("Not Monitored") represent cases where WAAS has insufficient measurements to guarantee the integrity of the ionosphere correction at an IGP. In this case, the ability of WAAS users to derive bounded ionosphere error sigmas for nearby IPPs is governed by Section A.4.4.10.3 of the WAAS MOPS [7]. Briefly, that section allows users to interpolate its ionosphere correction and UIVE for a given satellite from three surrounding IGPs instead of four if one (and only one) of the four has a GIVE of "Not Monitored". In this case, interpolation from three IGPs is allowed if a triangle formed from the corners of the three IGPs that do not report "Not Monitored" encloses the IPP for the satellite in question. The LAM should use the same algorithm to determine whether or not it can derive a valid UIVE in this situation. Fig. 9 illustrates an example of this situation. If an acceptable triangle cannot be formed or if more than one IGP has a GIVE of "Not Monitored", then the UIVE is not defined. For this reason, the UIVE decision rule, (12), includes a conditional statement that excludes any satellite for which the IPP flag is deemed "invalid."

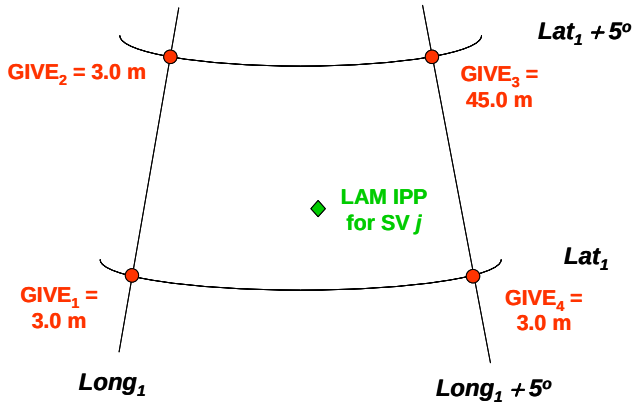

Fig. 8. Example of GIVE Values which Require IPP Exclusion but Generate Small LAM UIVE

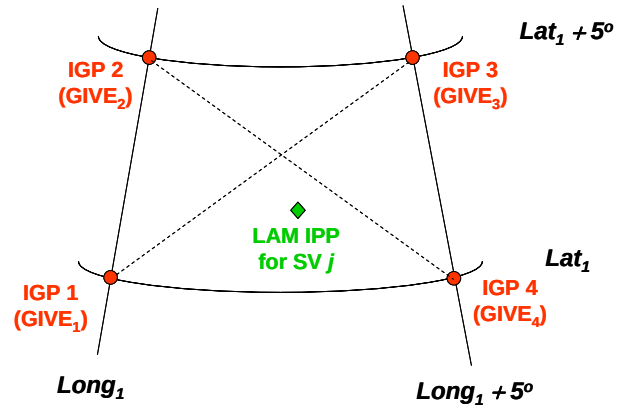

Fig. 9. LAM IPP for which Valid UIVE can be derived if either IGP 2 or IGP 3 is "Not Monitored"

B. UDRE Monitor Integrity

For Hazardous Misleading Information (HMI) to occur due to a CCD or SD failure, the WAAS monitor must fail to alert the user within the required alert time relative to when the actual navigation error exceeds the user protection level. In order to validate these timing and protection level requirements, this section draws on the time-varying conditional risk analysis of [13]. In analyzing the WAAS CCC and SD monitors, it is convenient to introduce several subsections that describe the important parameters for conditional risk analysis.

1) Relative Detection Time (RDT): When a hazardous threat occurs, the LAM must provide a timely warning to the user. The allowed time preceding that warning is referred to as the Time-to-Alert (TTA). For Category I approach, the Time-to-Alert is six seconds from the onset of HMI, which occurs at the moment the faulted error exceeds the user protection level. This definition intentionally defines TTA relative to the time of HMI and not relative to the onset of the threat. If the duration between the onset of the threat and the moment of HMI is called the Time-to-Hazard (TTH), then the total time

allowed before the user must process the alarm message is TTA + TTH. In order to meet this requirement, the Time-to-Detect (TTD) the fault plus the actual Time-to-Transmit (TTT) the alert must not exceed this limit.

$$TTD + TTT \le TTH + TTA \tag{19}$$

In LAM, the TTT (10 seconds) exceeds the TTA (6 seconds). To preserve integrity, the LAM must make up the difference through rapid detection of the threat. The amount of time that the monitor must make up is called the Relative Detection Time (RDT) [13].

$$RDT = TTA - TTT = -4 \text{ second} \tag{20}$$

2) Integrity Risk Allotment: This section describes the integrity risk allotment and the prior probabilities for the CCD and SD threats. The risk allotments for each threat are a fraction of the total Category I integrity risk tree budget of 2×10^{-7} per 150 seconds. For both the SD and CCD threats equal allotments are assigned in the horizontal and vertical directions. Because the integrity risk is greater in the vertical direction, the fact that the allotments are equal implies that system integrity can be ensured simply by demonstrating vertical integrity. The system integrity tree assigns a vertical risk allotment, P_a, of 2×10^{-8} to SDM and 5.0×10^{-9} to CCD monitoring [10].

The risk allotment, P_a, must exceed the combined risk that a fault occurs, that the fault-induced error exceeds the user protection level, and that a fault alert fails to reach the user within the required RDT. Furthermore, the risk of a user filter restart must also be considered since SD faults are more hazardous under restart conditions, as described by (7), and since CCD faults may only introduce HMI after a tracking restart. Relevant event probabilities are noted with abbreviations: F, fault occurs; MD, monitor misses detection; PL, error exceeds protection level; R, user carrier-smoothing filter undergoes a hazardous restart; NR, user filter undergoes no restart or a non-hazardous restart.

$$\begin{aligned} P_{MD} &= P\left(MD \mid PL, NR, F\right) \\ P_{PL} &= P\left(PL \mid NR, F\right) \\ P_R &= P(R \mid F) \\ P_{NR} &= P(NR \mid F) = 1 - P_R \approx 1 \end{aligned} \tag{21}$$

The allotment allowed by the LAM integrity tree for either CCD or SD must exceed the associated conditional risks:

$$P_a \ge \left(P_{MD} P_{PL} P_{NR} + P_R\right) P_F \,. \tag{22}$$

Table 2 summarizes the risk parameters for (22) associated with the CCD fault; Table 3, with the SD fault. Values in each table are justified in the remainder of Section VI.

TABLE 2. SUMMARY OF CCD EVENT PROBABILITIES

	Description	Value
P_A	Integrity Allotment for CCD	5.0×10^{-9}
P_F	Risk of CCD on any visible satellite per 150 s	1.1×10^{-6}
P_R	Risk of hazardous user restart	2.8×10^{-3}
$P_{LOI} = P_{MD}\, P_{PL}$	Risk of missed detection when error exceeds protection level	1.7×10^{-3}

TABLE 3. SUMMARY OF SD EVENT PROBABILITIES

	Description	Value
P_A	Integrity Allotment for SDM	2×10^{-8}
P_F	Risk of SD on any visible satellite per 150 s	2×10^{-6}
P_R	Risk of hazardous user restart	7×10^{-4}
$P_{LOI} = P_{MD}\, P_{PL}$	Risk of missed detection when error exceeds protection level	9×10^{-3}

3) Restart Probability, P_F: The LAM does not use the standard LAAS fault prior probability [14]. Rather, the LAM analysis uses a P_F derived empirically using the methods described in [9] and [15].

4) Restart Probability, P_R: When a user receiver starts or restarts tracking for a particular satellite, carrier-smoothing is reinitialized. If such a restart occurs shortly after an SD event, then the navigation solution is immediately affected by the full SD error. In the case of a CCD fault, no hazard will result unless a user-filter restart also occurs.

Not all user starts or restarts are hazardous. The restart probability, P_R, describes the likelihood of only those restart events which might cause HMI. Restart events which retain full integrity are lumped in with the non-hazardous restart (NR) classification. In fact, most tracking starts and restarts are non-hazardous because they occur during the time before the ground receiver has first approved the satellite. According to the requirement of Section V, the LAM ground facility cannot approve any satellite which has not been tracked for a 200 s duration. Even restart events that occur for moderate or high-elevation satellites (because of a cycle slip or an aircraft maneuver) may be classified as NR, as long as their associated errors do not exceed the protection level and result in a monitor missed detection. In fact, as demonstrated later in this section, only a certain range of user restart times pose an integrity hazard.

The hazardous restart probabilities, P_R, described by Table 2 and Table 3 are defined based on an assumed maximum window of hazardous restart times, W, equal to 60 s for SD faults and 240 s for CCD faults. The relationship between W and P_R is described by the following equation, which estimates the rate of user restarts (that occur outside the 200 s window allowed for ground approval) to be once per day per channel.

$$P_R = W\left(24\ \frac{\text{hour}}{\text{day}}\cdot 3600\ \frac{\text{seconds}}{\text{hour}}\right)^{-1} \tag{23}$$

5) Monitor Probability of Missed Detection, P_{MD} : The WAAS CCC and SD monitors detect faults with a bounded missed-detection risk, P_{MD}. This risk is a function of time, since the filtered monitor statistic generally grows larger as a function of time from the onset of the fault event. The P_{MD} transient is identical for WAAS and for LAM, except that the transient is delayed in the case of LAM by the RDT.

P_{MD} is related to the relative size of the expected monitor statistic $m(t)$, the monitor threshold T, and the monitor noise level σ_{mon}. These parameters were defined in Section III by (8) – (11). Assuming Gaussian overbound statistics, P_{MD} can be defined as follows by using a Q function, which describes the cumulative distribution function for a Normal distribution. Note that the missed detection probability is shifted in time by the RDT.

$$P_{md}(t-RDT) = Q\left(\frac{T-m(t)}{\sigma_{mon}}\right) - Q\left(\frac{-T-m(t)}{\sigma_{mon}}\right) \tag{24}$$

This equation represents the area of the Gaussian probability distribution integrated between positive and negative thresholds. A graphical representation of P_{MD} is depicted in Fig. 10. As the deterministic component of the monitor metric, $m(t)$, grows larger than the threshold, the area of the integral becomes vanishingly small.

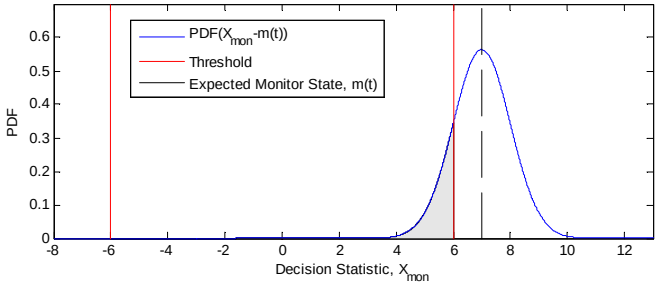

Fig. 10. Graphical Representation of P_{MD}

6) Vertical Protection Level: For HMI to occur the fault-induced error must exceed the user error bound called the protection level. Because the random component of the monitor transient is independent from the fault-free user error the probability of error exceeding the protection level, P_{PL}, is independent from the missed-detection probability, P_{MD} [13].

Because the vertical integrity requirements are stricter than the horizontal, only the Vertical Protection Level (VPL) need be considered. In LAM, the VPL is usually equal, and never less than, the user-evaluated expression for the fault-free (H0) case. This fault-free expression is labeled VPL_{H0}. In LAM, by design, the user VPL is also always at least as large as a second error expression labeled VPL_{LAM}. This expression reflects local monitor operation, which estimates the discrepancy between local measurements and WAAS corrections. Since the user VPL is equal to or larger than both the VPL_{H0} and VPL_{LAM} expressions, either expression may be used to evaluate P_{PL}. In general, the VPL_{H0} expression provides more tolerance for large unobservable errors; however, the VPL_{LAM} error bound offers the advantage that it tolerates larger observable errors and that it places no requirements on the integrity of the assumed WAAS error distribution.

LAM makes use of both the VPL_{H0} and VPL_{LAM} error bounds. The VPL_{H0} expression incorporates a K_{ffmd} factor which represents the sigma multiple bounding the risk level permitted for fault-free navigation. The K_{ffmd} parameter value is specified by the LAAS Interface Control Document (ICD) [16]. The sigma for the vertical navigation error, $\tilde{\sigma}_v$, is the root-sum-of-squares of the broadcast pseudorange error sigmas, $\tilde{\sigma}_{pr,i}$, weighted by the linearized vertical-position solution coefficients, $S_{v,i}$.

$$VPL_{H0} = K_{ffmd}\tilde{\sigma}_v \tag{25}$$

$$\tilde{\sigma}_v = \sqrt{\sum_i S_{v,i}^2\tilde{\sigma}_{pr,i}^2} \tag{26}$$

The VPL_{LAM} expression is similar to the VPL_{H0} equation, with a reduced K-factor, K_{bnd}, defined by the LAM integrity tree [10], and a sigma based on the actual error rather than the broadcast error sigmas. In addition, VPL_{LAM} incorporates a "decision-statistic" term, DS, which describes the local monitor's assessment of the quality of the WAAS corrections.

$$VPL_{LAM} = K_{bnd}\sigma_v + |DS| \tag{27}$$

$$\sigma_v = \sqrt{\sum_i S_{v,i}^2\sigma_{pr,i}^2} \tag{28}$$

The decision statistic is the sum of the WAAS discrepancies, δ_i, measured for each satellite.

$$DS = \sum_i S_{v,i}\delta_i \tag{29}$$

These discrepancy values difference the WAAS corrected pseudorange measurement, CPR_i, and the known range between the satellite and the LAM ground facility, R_i.

$$\delta_i = CPR_i - R_i \tag{30}$$

7) Probability of a Protection Level Violation, P_{PL}: Under faulted conditions, CCD and SD errors are modeled as deterministic, transient biases, $E(t)$, superposed with fault-free Gaussian noise. This error can be compared to either of the two protection level expressions defined in the previous section, VPL_{H0} or VPL_{LAM}, since the aircraft uses a VPL that is as large as or larger than either of these expressions.

Deriving P_{PL} using the VPL_{H0} expression requires a bound on the fault-free WAAS user error per satellite, described by a Gaussian sigma, $\sigma_{true,i}$ [11]. Using this user error bound, the one-tail probability that the WAAS error exceeds VPL can be expressed in terms of a Q function. Here, the deterministic ranging error, $E(t)$, is projected through the sensitivity weighting, S_k, for the faulted satellite, k.

$$P_{pl} = Q\left(\frac{-VPL_{H0} + \left| S_{v,k} E(t) \right|}{\sqrt{\sum_i S_{v,i}^2 \sigma_{true,i}^2}} \right) \tag{31}$$

In order to simplify this equation, it is convenient to substitute the R_{max} parameter for $\sigma_{true,i}$ using the notation of (16).

$$\sqrt{\sum_i S_{v,i}^2 \sigma_{true,i}^2} \le R_{max} \tilde{\sigma}_v \tag{32}$$

Applying bound (32) and definition (31), the following P_{PL} results.

$$P_{pl} \le Q\left(\frac{-K_{ffmd} \tilde{\sigma}_v + \left| S_{v,k} E(t) \right|}{R_{max} \tilde{\sigma}_v} \right) \tag{33}$$

This equation represents the risk of exceeding VPL_{H0}.

It is also possible to derive P_{PL} using VPL_{LAM}. This approach distinguishes between observable errors, which appear in DS, and unobservable errors, which do not appear in DS. The total vertical error, E_v, is the sum of the observable error, $E_{v,o}$, and the unobservable, $E_{v,u}$.

$$E_v = E_{v,o} + E_{v,u} \tag{34}$$

The LAM decision statistic, DS, estimates the vertical observable error subject to monitoring noise. This error is bounded by the normal distribution, $\mathcal{N}$, with deviation, σ_v [9].

$$p(DS) = \mathcal{N}\left(E_{v,o}, \sigma_v \right) \tag{35}$$

The fault is not hazardous if VPL_{LAM} exceeds the total vertical error. An expression for this integrity condition is

$$VPL_{LAM} = K_{bnd} \sigma_v + \left| DS \right| \ge \left| E_{v,o} + E_{v,u} \right| . \tag{36}$$

Applying the triangle inequality, a stricter form of this condition may be derived.

$$\left| DS \right| \ge \left| E_{v,o} \right| + \left| E_{v,u} \right| - K_{bnd} \sigma_v \tag{37}$$

Based on the probability distribution (35), the one-tail risk that condition (37) is not met is

$$P_{pl} \le Q\left(-K_{bnd} + \frac{\left| E_{v,u} \right|}{\sigma_v} \right) . \tag{38}$$

Because of the low probability of a satellite fault, the unobservable error need only be considered on a single satellite. Thus the unobservable vertical error may be expressed in terms of the unobserved ranging error, $E_u(t)$, for a single faulted satellite.

$$P_{pl} \le Q\left(-K_{bnd} + \frac{\left| S_{v,k} E_u(t) \right|}{\sigma_v} \right) \tag{39}$$

In both the VPL_{H0} and VPL_{LAM} cases, (33) and (39), geometry can be removed from the P_{PL} expression by finding the worst-case value of P_{PL} over all geometries. In both cases this worst-case occurs when the random error on the faulted satellite dominates over all other random error terms [13], [17]. In this case, the P_{PL} expressions may be simplified as follows.

$$P_{pl} \le Q\left(\frac{-K_{ffmd} + \left| E(t) \right| / \tilde{\sigma}_{pr,k}}{R_{max}} \right) \quad \text{for } \mathrm{VPL_{H0}} \tag{40}$$

$$P_{pl} \le Q\left(-K_{bnd} + \left| E_u(t) \right| / \sigma_{pr,k} \right) \quad \text{for } \mathrm{VPL_{LAM}} \tag{41}$$

8) *Loss of Integrity Risk, P_{LOI}* : For a loss of integrity to occur, the product $P_{MD}P_{PL}$ must not exceed the risk allocation specified by Table 2 and Table 3. This risk allocation is referred to as the Loss of Integrity Probability, P_{LOI}. The P_{LOI} requirement can either be evaluated as a probability test or as a test based on the Maximum Allowable Error in Range (MERR) as described in [13]. Both tests are equivalent.

As a first step in testing that the product $P_{MD}P_{PL}$ does not exceed P_{LOI}, it is convenient to consider cases in which no user-filter restart occurs. In these cases, SD faults can cause HMI, but CCD faults cannot. To validate monitor integrity, $P_{MD}P_{PL}$ must be tested for every threat in the SD threat space. This computation is significantly simplified using the MERR methodology of [13], which allows direct computation of the worst allowable steady-state error, E_{ss}, for any value of the monitor statistic, m_{ss}. The resulting contour is plotted for UDRE ≤ 8 (all elevations) in Fig. 11 and for UDRE ≤ 11 (low elevations) in Fig. 12. Because the MERR contour is greater than all the threat points on this plot of E_{ss} vs. m_{ss}, integrity is verified for all threats in the SD threat space at least for all cases without a user-receiver restart.

To complete the threat analysis, $P_{MD}P_{PL}$ must also be assessed considering user filter restarts. The space of user filter restarts is described by the restart time, t_a. This parameter describes the time difference from the initial occurrence of the fault to the moment at which the user receiver re-initializes tracking on the faulted satellite. Since the user filter is required to converge to the nominal filter within 100 s, the lowest restart time which need be considered is t_a = -100 s, which corresponds to the case in which the user filter converges at the same moment the fault occurs. The largest relevant value of t_a corresponds to the moment (time shifted by the RDT) at which P_{MD} falls equal or below P_{LOI}. After this moment, labeled t_{max}, the monitor assumes full responsibility for user integrity. For values of t_a larger than t_{max}, the user receives an alert immediately after the restart occurs, such that no HMI results. Hence, the limits for t_a are the following.

$$-100 \le t_a \le t_{max} \tag{42}$$

Restart events for which $P_{MD}P_{PL}$ does not exceed the P_{LOI} allocation are grouped in the NR category, which describes both non-hazardous restarts and non-restart faults. Cases for which $P_{MD}P_{PL}$ exceeds P_{LOI} for some period of time are deemed hazardous restarts and placed in the R category. In this manner, restart threats can be classified as either R or NR.

Fig. 13 - Fig. 15 classify the threat space for SD and CCD by category (NR or R). The first two of these figures illustrate the SD threat space for the case of UDRE ≤ 8, all elevations (Fig. 13) and the case of UDRE ≤ 11, low elevations (Fig. 14). Although the full threat description is three dimensional, consisting of E_{ss}, m_{ss}, and t_a, these plots represent the NR and R classifications in two-dimensions, by illustrating the worst error for all possible values of monitor statistic, m_{ss}. Fig. 15 illustrates the threat space for the CCD fault. In contrast with the SD fault, the parameter space describing CCD faults is unbounded, as the divergence parameter, d, can take any positive value.

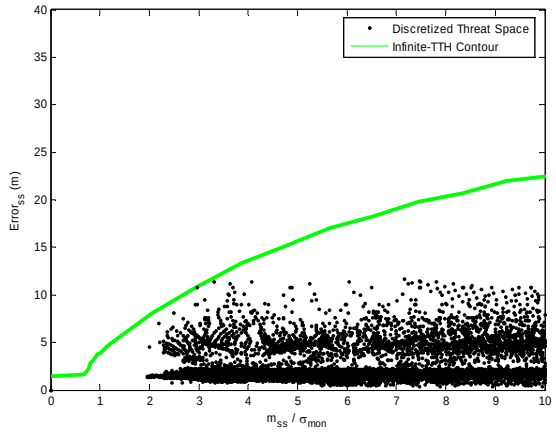

Fig. 11. Integrity for SD with UDREI ≤ 8, All Elevations, No Restart

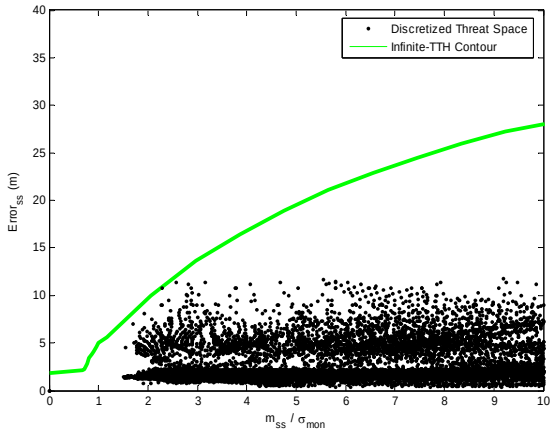

Fig. 12. Integrity for SD with UDREI ≤ 11, Elevations to 38°, No Restart

9) Hazardous Restart Window, W: The probability of a hazardous restart was derived assuming a bound, *W*, on the window of hazardous restart times. For SDM, the upper bound on *W* was taken to be 60 s. As seen in Fig. 13, the shaded window of hazardous restarts, R, has a 21 seconds duration (-5 s ≤ t_a ≤ 16 s). From Fig. 14, the window of hazardous restart events has a duration of 24 seconds (-6 s ≤ t_a ≤ 18 s). Thus for both UDRE cutoffs, the width of the R region meets the *W* requirement by a factor of more than two.

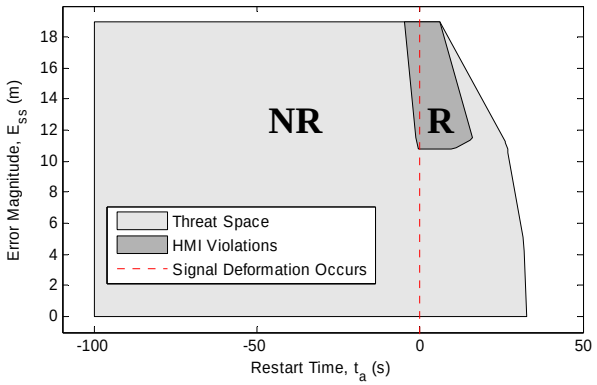

Fig. 13. Classification of SD Threats with Restart and UDREI ≤ 8

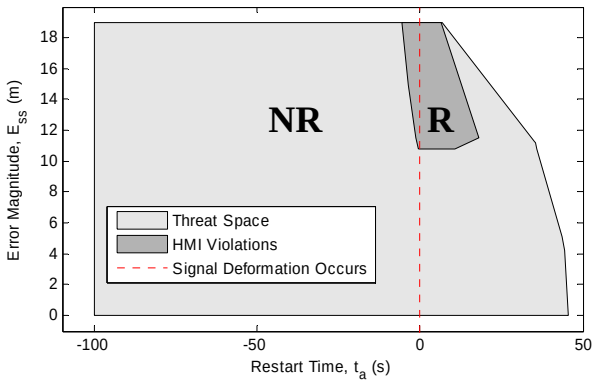

Fig. 14. Classification of SD Threats with Restart and UDREI ≤ 11

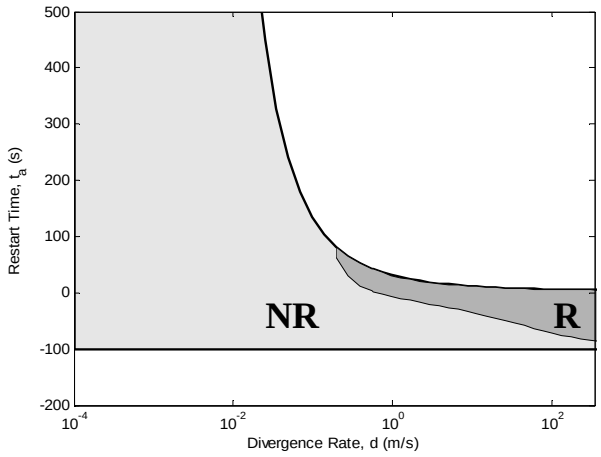

Fig. 15. Classification of CCD Threats as NR or R

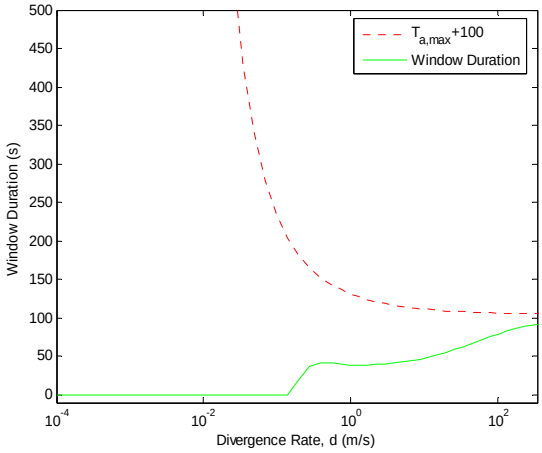

Fig. 16. Duration of Hazardous Restart Window for CCD Threats

For CCD, the upper bound on W was taken to be 240 s. Fig. 15 shows that the restart window stretches as wide as 93 s at the far left of the plot, where d = 400 m/s. Although the window of hazardous restarts worsens for higher values of d, it cannot be larger than 100 + t_{max}, the range allowed for the t_a parameter according to (42). As evidenced by Fig. 15 and Fig. 16, this upper bound on the hazardous restart time decreases with increasing d. Thus, the window of hazardous restarts cannot exceed 100 + t_{max} evaluated at the right hand side of the figures (d = 400 m/s). At this point, 100 + t_{max} = 107 s. Thus for the CCD fault mode, the maximum length restart window is at most 107 s, which is better than a factor of two below the 240 s requirement.

Since all risk budgets outlined in Table 2 and Table 3 are met for the SD and CCD threat space, the combined risk probabilities satisfy (22). Accordingly, the integrity of the UDREI monitor, (13), is validated for all threats in the SD and CCD threat spaces.

VII. AVAILABILITY IMPACT

As shown in the previous section, the UDRE and UIVE monitors, (12) and (13), provide full integrity for LAM users through ionosphere, CCD and SD faults. Unfortunately, the UIVE and UDRE parameters are not direct indicators of WAAS monitor performance. Both the UDRE and UIVE parameters may increase because of poor data quality or because of other WAAS real-time monitoring. For this reason, the application of the LAM UIVE and UDRE monitors results in a significant number of false positive detections. These false positives have a detrimental impact on the continuity and availability that can be achieved by LAM.

A set of nine normal days were investigated to assess the false-detection performance of the UIVE and UDRE monitors. These data were acquired by the William J. Hughes FAA Technical Center in Atlantic City, NJ.

On typical days, UIVE monitor detections generally occurred for satellites at low elevations, where WAAS had insufficient data to verify ionosphere conditions. This effect is particularly pronounced on the East Coast of the United States, where many rising satellites are observed and where the coverage of the WAAS ionosphere grid is sparse.

UDRE monitor detections generally occurred for satellites at high elevations, when anomalous UDRE spikes were observed in the WAAS data. Characteristic high-elevation UDRE spikes are illustrated in Fig. 17. A UDRE monitor alert occurs whenever the solid blue curve (received UDREI parameter) exceeds the dashed red curve (UDREI threshold for the satellite in question). UDREI spike anomalies have been observed and discussed by the WAAS Integrity Performance Panel. These spikes are not necessary to ensure WAAS integrity and may be fixed in an optional WAAS upgrade. Although these spikes have a negligible impact on WAAS performance, they result in a non-negligible continuity and availability penalty for LAM.

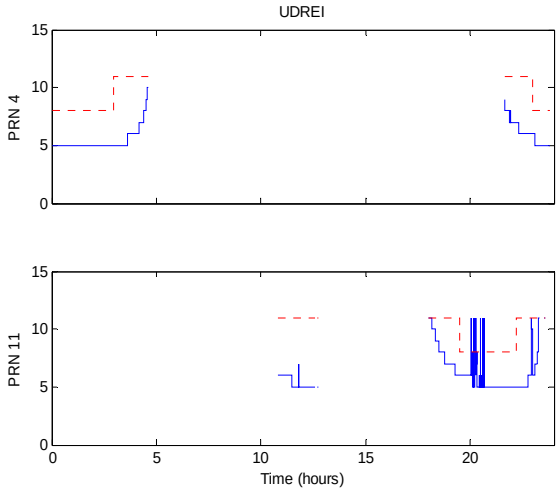

Fig. 17. Normal UDREI Data (PRN 4) and UDREI Spikes (PRN 11)

The availability impact of false detections can be described indirectly by computing the number of epochs for which the UIVE and UDRE monitors trigger an alarm. The statistics for the nine nominal days of data are depicted graphically by means of two dimensional histograms in Fig. 18 and Fig. 19. The UIVE histogram displays 1 Hz data for all satellites as a function of UIVE value and satellite elevation. The UDREI histogram displays 1 Hz data for all satellites as a function of UDREI value and satellite elevation.

In both figures, the LAM cutoff is superimposed on the histogram as a solid red line. A significant number of epochs exceed both the UDREI and UIVE cutoffs. In all, the fraction of epochs exceeding the UDREI cutoff was 0.001. The fraction of epochs exceeding the UIVE cutoff was 0.006. Thus in 7 out of 1000 epochs, LAM satellite geometry is slightly worse than nominal, since one or more satellites is excluded by the UDRE or UIVE monitors. This information should be used to update the availability predictions of [1] and [2].

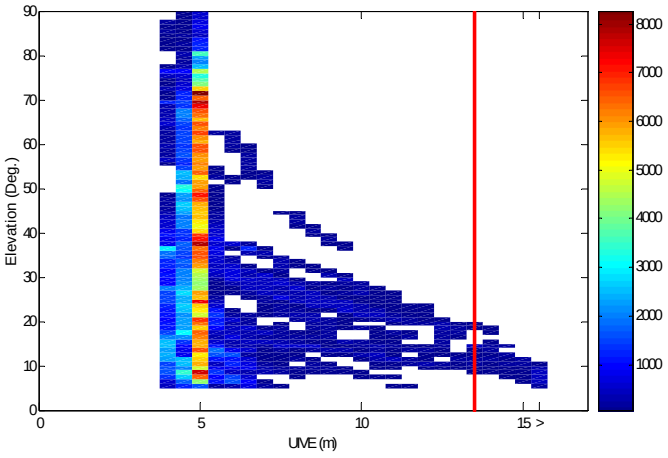

Fig. 18. Histogram of UIVE and Elevation over Nine Nominal Days

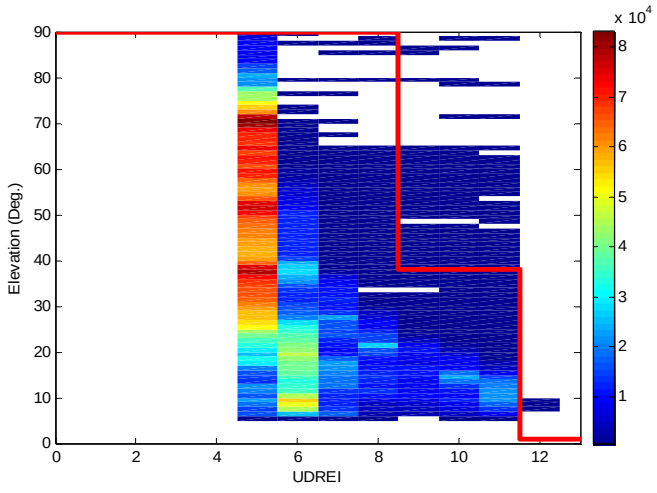

Fig. 19. Histogram of UDREI and Elevation over Nine Nominal Days

Continuity risk is also impacted by the UIVE and UDRE monitors; however, the continuity effect is assessed only once per each period in which UIVE or UDREI parameters continuously exceed the cutoffs, (12) or (13). The number of continuous satellite outage periods initiated by the UIVE monitor was 86 and by the UDRE monitor was 203. Most of these outages lasted for periods of longer than 20 s. The total number of configuration changes (289) in which a satellite was abruptly removed from the constellation corresponds to a configuration change risk of 5.6×10^{-3} per 15 second. This configuration change risk is substantially higher than that normally assumed for satellite outages in conventional LAAS. To handle the continuity impact of a configuration change for LAM users, it may be necessary to either set the number of allowed critical satellites to zero or to compute continuity based on average risk rather than specific risk.

VIII. SUMMARY

This paper demonstrates the validity of using WAAS monitoring to establish integrity for fault modes which are not otherwise observable using local airport monitoring. These fault modes include anomalous ionosphere gradients, satellite code-carrier divergence failures and satellite signal deformation failures. These threats are protected respectively by the ionosphere storm detector, code-carrier coherence and signal deformation monitors that exist in WAAS or that will be available in WAAS by 2008.

By applying a threshold to two WAAS broadcasts parameters, User Ionosphere Vertical Error (UIVE) and User Defined Ranging Error (UDRE), LAM guarantees that WAAS thresholds are sufficient to ensure the integrity of protection level and time-to-alert requirements for Category I. A conditionally risk analysis validates that these UIVE and UDRE monitors ensure LAM integrity even taking into account that the total transmission time for LAM (10 s) exceeds the allowed time-to-alert for Category I (6 s). The major drawback of the UDRE and UIVE monitors is an availability (and possibility a continuity) penalty which results from LAM false detections, as observed in nine days of field data acquired under nominal conditions.

ACKNOWLEDGEMENTS

The authors gratefully acknowledge the Federal Aviation Administration Satellite Navigation LAAS Program Office (AND-710) for supporting this research. We also thank Curtis Shively and Ranjeet Shetty for their editorial advice in preparing these concepts for inclusion in the Local Airport Monitor Algorithm Description Document. The opinions discussed here are those of the authors and do not necessarily represent those of the FAA or other affiliated agencies.

REFERENCES

[1] C. Shively, R. Niles, and T. Hsiao, "Performance and availability analysis of a simple local airport position domain monitor for WAAS," *Proc. of Institute of Navigation GNSS 2005*, pp. 2837-2854.

[2] J. Rife, S. Pullen, T. Walter and P. Enge, "Vertical protection levels for a local airport monitor for WAAS," *Proc. of Institute of Navigation Annual Meeting 2005*, pp. 745-758.

[3] S. Datta-Barua, T. Walter, S. Pullen, M. Luo, J. Blanch, and P. Enge, "Using WAAS ionospheric data to estimate LAAS short-baseline gradients," *Proc. of Institute of Navigation National Technical Meeting 2002*, pp. 523-530.

[4] M. Luo, S. Pullen, S. Datta-Barua, G. Zhang, T. Walter, and P. Enge, "LAAS study of slow-moving ionosphere anomalies and their potential impacts," *Proc. of Institute of Navigation GNSS 2005*, pp. 2337-2349.

[5] R.E. Phelts, T. Walter, and P. Enge, "Toward real-time SQM for WAAS: improved detection techniques," *Proc. of the Institute of Navigation GPS 2003*, pp. 2739-2749.

[6] RTCA Inc, *Minimum Operational Performance Standards for GPS Local Area Airborne Equipment*, RTCA/DO-253A, November 28, 2001.

[7] RTCA Inc, *Minimum Operational Performance Standards for GPS/Wide Area Augmentation System Airborne Equipment*, RTCA/DO-229C, November 28, 2001.

[8] M. Luo, S. Pullen, A. Ene, D. Qiu, T. Walter, and P. Enge, "Ionosphere threat to LAAS: updated model, user impact, and mitigations," *Proc. of the Institute of Navigation GNSS 2004*, pp. 2771-2785.

[9] FAA, *Algorithm Description Document for Local Airport Monitor*, FAA, March 3, 2006.

[10] C. A. Shively, "Ranging source fault integrity concepts for a local airport monitor for WAAS," *Proc. of the Institute of Navigation National Technical Meeting 2006*, pp. 413-431.

[11] R. Niles and C. A. Shively, "Development of an Error Model for Locally-Achieved Performance of WAAS," *Proc. of the Institute of Navigation National Technical Meeting 2006*, pp. 342-357.

[12] S. Pullen, M. Luo, and J. Rife, "Ionosphere anomaly impact on local area monitoring (LAM)," unpublished presentation to FAA at LAM progress meeting in Rosslyn, VA, June 14, 2005.

[13] J. Rife and R. E. Phelts, "Formulation of a time-varying maximum allowable error for ground-based augmentation systems," *Proc. of Institute of Navigation National Technical Meeting 2006*, pp. 441-453.

[14] FAA, *Specification: Category I Local Area Augmentation System Ground Facility*, FAA-E-2937A, April 17, 2002.

[15] S. Pullen, J. Rife, and P. Enge, "Prior probability model development to support system safety verification in the presence of anomalies," *IEEE/ION Position, Location and Navigation Symposium*, 2006.

[16] RTCA Inc, *GNSS-Based Precision Approach Local Area Augmentation System (LAAS) Signal-in-Space Interface Control Document (ICD)*, RTCA/DO-246B, November 28, 2001.

[17] T. Zaugg, "A new evaluation of maximum allowable errors and missed detection probabilities for LAAS ranging source monitors," *Proc. of the Institute of Navigation Annual Meeting 2002*, pp. 187 - 194.